

Facile bulk preparation and structural characterization of agglomerated γ - $\text{Fe}_2\text{O}_3/\text{SiO}_2$ nanocomposite particles for nucleic acids isolation and analysis

Valentin Natarov^{a,b,*}, Dzmitry Kotsikau^a, Vladimir Survilo^b, Andrei Gilep^c, Vladimir Pankov^a

^a Department of Chemistry, Belarusian State University, 4 Nezavisimosti Av., 220030, Minsk, Belarus

^b JSC «GenTerra», 9/1 Godovikova St., 129085, Moscow, Russian Federation

^c Institute of Bioorganic Chemistry, National Academy of Sciences of Belarus, 5/2 Kuprevicha St., 220141, Minsk, Belarus

HIGHLIGHTS

- γ - $\text{Fe}_2\text{O}_3/\text{SiO}_2$ nanocomposites were synthesized via two sol-gel methods.
- Silanization and calcination provide structural stability to the obtained materials.
- The nanocomposites have demonstrated similar effectiveness of DNA isolation.
- The isolated nucleic acids are pure enough to be used for molecular biology.

ARTICLE INFO

Keywords:

Magnetic particles
Bioseparation
Silica
Nucleic acids
Sol-gel synthesis

ABSTRACT

Two facile methods for bulk preparation of γ - $\text{Fe}_2\text{O}_3/\text{SiO}_2$ agglomerated magnetic nanocomposite (MNC) particles for magnetic separation of nucleic acids (NAs) are compared together. Different silica coating approaches were used for iron oxide silanization: Stöber method and sodium silicate dense-liquid process. Additional thermal treatment at 750 °C provided thermal and structural stability to the MNCs. The structural characteristics, magnetic properties, size and morphology of the synthesized materials have been studied. To validate the synthesized materials, the MNCs were used for the isolation of nucleic acids from human buccal epithelium cells and two human biosamples (whole blood and plasma) with addition of pathogenic viruses. It was shown that the prepared near-micron sized agglomerates of superparamagnetic ($M_s = 40$ –45 emu/g) γ - $\text{Fe}_2\text{O}_3/\text{SiO}_2$ MNC particles are fully coated with silica. The synthesized materials combine the advantages of nanosized (superparamagnetism) and micron-sized objects (separability, average precipitation stability). Both types of the MNCs described in the paper have demonstrated similar effectiveness of NAs isolation, comparable with commercial MAGNO-sorb[®] total NAs isolation kit (InterLabService, Russia) used as a reference. The appropriate structural stability, high magnetization and proper purity of the isolated NAs (A260/A280 ratio near 1.9) make the studied MNCs promising materials for magnetic bioseparation.

1. Introduction

In the past decade, colloidal magnetic nanocomposites (MNCs) based on iron oxide (Fe_3O_4 , γ - Fe_2O_3) and silica (SiO_2) have attracted a considerable attention due to a wide range of their applications such as electromagnetic radiation protection [1], water purification from heavy metals and dyes [2], separation and purification of biomolecules [3,4], magnetic resonance imaging [5], radio-frequency hyperthermia [6], biosensing and targeted drug delivery [7]. Biomedical use of silica-coated MNCs is especially attractive due to their facile synthesis, chemical and aggregation stability, hydrophilic character, biocompatibility

and easily functionalizable surface [6]. MNC particles, which are characterized by a combination of a suitable colloidal stability in aqueous dispersions, a high magnetic response (time required for isolation of MNCs from solution with external magnetic field) and a functionalized surface, are of great interest for magnetic separation and purification of biomolecules (nucleic acids, proteins, cells etc.) [3,4]. Generally, magnetic bioseparation technique is based on selective adsorption of biomolecules on the surface of MNC particles and further isolation of a magnetic sorbent conjugated with biomolecules from initial solution using a permanent magnet. After desorption, pure and concentrated samples of biomolecules can be used for further

* Corresponding author. JSC «GenTerra», 9/1 Godovikova St., 129085, Moscow, Russian Federation.

E-mail address: v.natarov@genterra.ru (V. Natarov).

<https://doi.org/10.1016/j.matchemphys.2018.08.011>

Received 3 April 2018; Received in revised form 30 July 2018; Accepted 7 August 2018

Available online 09 August 2018

0254-0584/ © 2018 Elsevier B.V. All rights reserved.

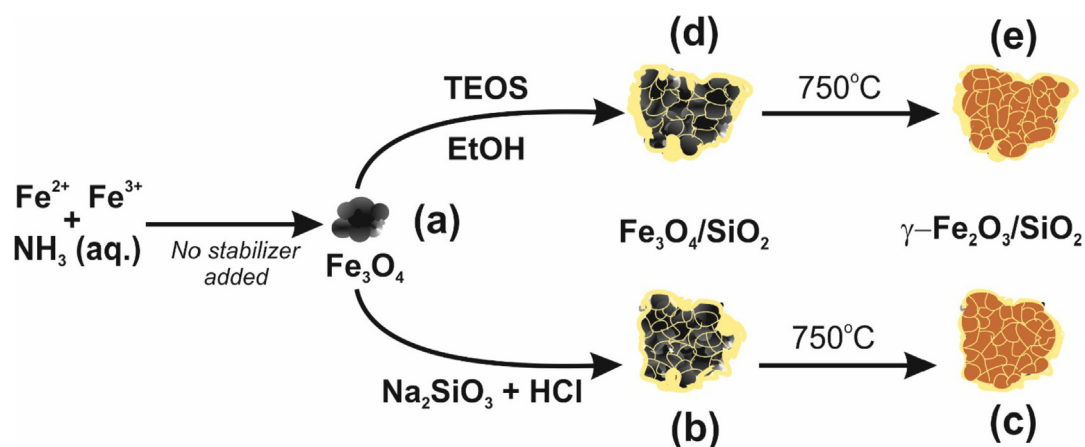


Fig. 1. Schematic illustration of the MNCs preparation via different silanization approaches.

operations [3]. Despite the presence of a variety of other purification techniques like spin-column chromatography, liquid-phase extraction, ultrafiltration etc., magnetic bioseparation remains to be a popular method, especially for nucleic acids (NAs) isolation. The method is of great interest since it implies quick, easy and user-friendly protocols, and allows avoiding the centrifugation step required in case of non-magnetic sorbents [8]. Moreover, the MNCs can be used with automatic stations for NAs isolation simplifying significantly routine research procedures, forensic or large-scale clinical analysis [9].

The isolation of NAs from biological specimens is an integral part of any experiments in molecular biology, biotechnology and medical diagnostics [3,8]. After polymerase chain reaction (PCR) assay had become a powerful tool in clinical analysis, forensic science and research in biosciences, great attention was paid to protocols for DNA purification. R. Boom et al. reported a facile protocol for the isolation of PCR-acceptable NAs using amorphous silica particles and guanidine thiocyanate acting as a chaotropic agent [10]. Nowadays, the “magnetic modification” of the Boom method, where silica coated magnetic beads are used instead of single SiO_2 material, is popular and well-proven technique [11]. A possible mechanism of NAs interaction with MNCs has been described by Xu et al. [12].

A number of synthetic strategies for MNCs preparation has been proposed. Among them are chemical precipitation (sol-gel technology), solvothermal method, microemulsion synthesis, aerosol spray pyrolysis etc. [13–15]. Despite the advantages of all the mentioned above methods providing better monodispersity control, sol-gel approach remains to be the most economically reasonable for bulk scaling. Among the wide range of magnetic materials, iron oxide is the most frequently used for the preparation of MNCs due to its simple preparation method and room temperature formation. However, magnetite nanoparticles obtained via co-precipitation method have a typical size of 5–10 nm, which results in the formation of a rather stable sol, making impossible the complete magnetic separation of solid particles with adsorbed NAs. Instead of individual nanoparticles, we propose their agglomerates to coat by silica. The same approach was used by Fu et al. [16] to obtain highly monodisperse $\text{Fe}_3\text{O}_4/\text{SiO}_2$ composite particles from micelles of hydrophobic magnetite coated with oleic acid. A typical synthesis procedure includes two steps – synthesis of magnetic nanoparticles and their silica coating (silanization).

The use of hydrolysis of various tetraalkoxysilanes in ethanol media, mostly tetraethoxysilane (TEOS), is a well-studied method for silica coating [17,18]. However, there are some studies considering sodium silicate as a promising inorganic alternative to organosilanes, which is cheaper and environmentally friendly [19–22]. TEOS and sodium silicate were used by Liu et al. [23] to obtain individual and mixed-precursor silica coatings on magnetite nanoparticles. Jitianu et al. [24] compared TEOS and sodium silicate as silanization precursors.

However, their use for the preparation of silica to be applied for NAs bioseparation has not been studied. Tetraalkoxysilanes are relatively expensive and hazardous materials, which inhibits their commercialization. In contrast, sodium silicate is cheap and water-soluble silica source promising for commercial bulk preparation of low-cost magnetic NAs sorbent [22].

The aim of this work was to compare different methods of silica-coating for bulk preparation of agglomerated magnetic sorbent $\gamma\text{-Fe}_2\text{O}_3/\text{SiO}_2$ suitable for the isolation of PCR-acceptable NAs. The structural and magnetic features of the MNCs obtained via different silica precursors were studied. Special attention was paid to the influence of MNCs agglomeration on the NAs isolation effectiveness. Human biosamples with addition of pathogenic viruses (whole blood and blood plasma) and buccal epithelium cells were used as target subjects for NAs isolation. Commercially available MAGNO-sorb[®] total NAs isolation kit (InterLabService, Russia) was used as a reference to estimate the compliance of the synthesized materials with commercial standards of NAs isolation. The chosen PCR test-systems cover an important area of medical diagnostics of pathogenic viruses like hepatitis virus type B (HBV), hepatitis virus type C (HCV) and human immunodeficiency virus (HIV) [25]. To demonstrate the purity and quantity of isolated human genomic DNA, UV spectroscopy and PCR test-system specific for ACE gene I/D polymorphism detection were applied.

2. Experimental

2.1. Preparation of Fe_3O_4 nanoparticles

All the chemicals used in the work were of analytical grade. A schematic illustration of the synthesis and nomenclature of the synthesized materials is presented in Fig. 1. Briefly, Fe_3O_4 nanoparticles were obtained by combined hydrolysis of $\text{Fe}(\text{NO}_3)_3$ and FeSO_4 with ammonia solution at the first step. Then, Fe_3O_4 was coated with SiO_2 via two different methods – Stöber process and dense-liquid chemical process involving sodium silicate. At the final step, the samples were calcinated at 750°C .

Magnetite nanoparticles were prepared with a co-precipitation method [26]. Briefly, 900 mL of iron salts solution containing 0.24 M $\text{Fe}(\text{NO}_3)_3$ and 0.12 M FeSO_4 was mixed with 1850 mL of 1.4 M aqueous ammonia. The synthesis was carried out in a 5 L flask supplied with an effective mechanical stirrer for 2 h at 23°C . The obtained black precipitate was separated with a NdFeB permanent magnet and washed 5 times with distilled water to remove all the soluble products and the excess of ammonia.

2.2. Preparation of $\text{Fe}_3\text{O}_4/\text{SiO}_2$ and $\gamma\text{-Fe}_2\text{O}_3/\text{SiO}_2$ nanocomposites

The dense-liquid process [23] was used as an inorganic approach for silica coating. Briefly, 25 g of the freshly obtained Fe_3O_4 nanoparticles were suspended with ultrasonication in 1500 mL of distilled water with $\text{pH} = 10$ (adjusted with ammonia), and the suspension was heated to 70°C . Then, 900 mL of 0.25 M sodium silicate solution and 800 mL of 0.5 M HCl were added dropwise to the suspension. During the silica-coating process, pH was maintained around 10–12. The resulting suspension was additionally stirred (300 rpm) for 2 h at 70°C . The obtained precipitate was washed three times with distilled water and dried in vacuum.

A modified Stöber method [18,27] was used as the second way of silica coating. Briefly, 25 g of freshly obtained Fe_3O_4 nanoparticles were suspended with ultrasonication in 2 L of 70% ethanol with addition of 10 mL of 11 M ammonia. Then, 53 mL of freshly distilled TEOS was added dropwise to the suspension under stirring (400 rpm) at 25°C . After 24 h of constant stirring, the resulting grayish-black precipitate of MNCs was washed with 95% ethanol and distilled water followed by drying in vacuum at room temperature. Note that the as prepared MNCs suspensions and powders were denoted here as $\text{Fe}_3\text{O}_4/\text{SiO}_2$ samples since they had black color typical of magnetite (Fe_3O_4). The powdered samples of the MNCs obtained by both approaches were additionally calcined in a muffle furnace for 1 h at 750°C . The thermally treated samples were denoted as $\gamma\text{-Fe}_2\text{O}_3/\text{SiO}_2$ since they had brown color typical of maghemite ($\gamma\text{-Fe}_2\text{O}_3$). Saline suspensions of the obtained MNCs (10 mg/mL NaCl, 0.03% NaN_3) with the concentration of solids of 50 mg/mL were used for the isolation of NAs.

2.3. Characterization of nanocomposites

Scanning (SEM) and transmission (TEM) electron microscopy analysis was performed on Hitachi S-4800 and LEO 906E microscopes, respectively. The X-ray diffraction (XRD) patterns of the powdered samples were recorded on a DRON-2.0 diffractometer using Ni-filtrated $\text{Co K}\alpha$ radiation ($\lambda = 1.78896 \text{ \AA}$) in 2θ range of $20\text{--}80^\circ$. The thermal analysis (DSC, TG) was carried out on a NETZSCH STA 449C instrument at scanning rate $5^\circ\text{C}/\text{min}$ in temperature range $30\text{--}800^\circ\text{C}$. The Fourier transform infrared (FTIR) spectra were recorded in wavenumber range $400\text{--}4000 \text{ cm}^{-1}$ on a Thermo Nicolet Avatar 330 FTIR spectrometer supplied with a Smart Diffuse Reflectance Accessory. The hydrodynamic size and ζ -potential of the MNCs particles in aqueous medium were obtained by using a Malvern Zetasizer NanoZS instrument. The room temperature field-dependent magnetization curves were acquired using a Cryogen Free Measurement System (CFMS, Cryogenic Ltd.) in vibration sample magnetometer (VSM) mode. The nitrogen adsorption-desorption analysis of the powdered MNCs was carried out on a Micromeritics ASAP 2020 system.

2.4. Nucleic acids isolation and characterization

Schematic illustration of the DNA isolation protocols, which were used to validate the synthesized materials, is presented in Fig. 2. A typical isolation protocol is composed of the following steps: i) lysis of biomaterial; ii) incubation providing binding of NAs with sorbent; iii) several washings to remove impurities such as proteins or excess of guanidine; iv) elution (desorption) of NAs from sorbent into clear solution.

To prepare model biosamples, buccal epithelium cells from two different volunteers were centrifuged (4 min, 12000 rpm) from 1 mL of saline (0.9% NaCl) solution after 3 min of gargling. Briefly, 500 μL of lysis buffer (4 M Gu-HCl, 10 mM Tris-HCl, 10% i-PrOH, $\text{pH} = 4.9$) were added to the cells precipitate followed by 8 min shaking at room temperature. Then, 20 μL of MNCs saline suspension (50 mg/mL) were added. After 10 min of vortexing, the MNCs particles with immobilized DNA were collected by using an Invitrogen Capture-Tec™ magnetic stand, and the supernatant was removed. The particles were washed

twice with 70% EtOH and dried for 10 min. The NAs were eluted with 200 μL of TE buffer (10 mM Tris-HCl, 1 mM EDTA, $\text{pH} = 8.6$) at 70°C . The concentration and quality (A260/280 ratio) of the isolated NAs (DNA and RNA mix) were analyzed on a NanoDrop 2000c UV–vis spectrometer. Genomic DNA isolated from buccal epithelium cells was used for ACE gene I/D polymorphism PCR assay. The Ethics Committee of the Belarussian State University approved samples collection procedure and analysis.

The isolation of NAs from human plasma with HIV and whole blood with HCV-HIV-HBV viral mix was carried out with the manufacturer instructions described in MAGNO-sorb® total NAs isolation kit (InterLabService, Russia). The total concentration of viruses in each biological sample was equal to 10^3 IU/mL. Both the synthesized MNCs and the commercial sorbent were used.

To estimate the adsorption capacities of the MNCs in relation to NAs molecules, 10 μL of the MNCs suspension (25 mg/mL) were washed 2 times with water in a test tube. Then 50 μL of salmon genomic DNA solution (1560 ng/ μL , Sigma Aldrich) and 250 μL of lysis buffer were added. The tubes were kept at 25°C under shaking for 9 h. After separation of the MNCs from the liquid phase, the concentration of the non-sorbed DNA molecules was estimated with UV spectroscopy. To separate the DNA molecules sorbed on the solid phase, the MNCs were eluted 7 times with TE buffer, and the concentration of each solution was measured.

2.5. PCR amplification and agarose gel electrophoresis

PCRs assays were performed with specific primers for ACE gene I/D polymorphism (forward primer – CTGGAGACCACTCCCATCCTTTCT, reverse primer – GATGTGCCATCACATTCGTCAGAT) in total volume of 30 μL on a Bio Rad T 100 Thermal cycler. The ACE PCR mix ($\text{pH} = 8.3$) contained 50 mM KCl, 10 mM Tris-HCl, 1.5 mM MgCl_2 , 5.0 pmol of each primers and 200 μM of deoxyribonucleoside triphosphates (dNTPs). The thermal cycling protocol included initial denaturation at 95°C for 5 min, 34 cycles of amplification (denaturation at 94°C for 20 s; annealing at 58°C for 20 s, extension at 72°C for 45 s) and final elongation at 72°C for 10 min. The ACE PCR products were analyzed by electrophoresis in 1.5% agarose gel containing 0.25 $\mu\text{g}/\text{mL}$ ethidium bromide. TAE running buffer (10 mM Tris, 40 mM HAC, 1 mM EDTA, $\text{pH} = 8.0$) was used. Electrophoresis was carried out in a horizontal unit (Bio Rad) at 125 V for 40 min. The real-time PCR test for detection of viral DNA using AmpliSens® HVC-HIV-HBV diagnostic kit (Russia) and AmpliSens® HIV was carried out on a Rotor-Gene Q (QIAGEN) in accordance with the manufacturer instructions. Fluorescent signals were recorded during each annealing step of amplification cycles. After the amplification, cycle threshold (C_t) value have been assigned to each sample.

3. Results and discussion

3.1. Characterization of $\text{Fe}_3\text{O}_4/\text{SiO}_2$ and $\gamma\text{-Fe}_2\text{O}_3/\text{SiO}_2$ nanocomposites

The XRD patterns of all the samples are shown in Fig. 3. The peaks at 2θ values of about 35.0, 41.3, 50.5, 63.1, 67.4, 74.5 can be respectively indexed to the (220), (311), (400), (422), (511), (440) planes reflections of cubic-type spinel structure (space group Fd3m), characteristic for whether Fe_3O_4 or $\gamma\text{-Fe}_2\text{O}_3$ phases, which are thermodynamically untestable at room temperature. The XRD analysis does not allow the exact phase identifying taking into account the similarities of their crystalline structures and the broadness of the diffraction reflexes. One can suppose that the as prepared samples contain magnetite phase since have black color typical of Fe_3O_4 . The low intensity and diffuse shape of the peaks indicates a nanosized character of iron oxide. Also, it can be related to a poor crystallinity of iron oxide obtained at low temperature without additional calcination. Silica occurs in the MNCs in an X-ray amorphous state as evidenced by a broad peak

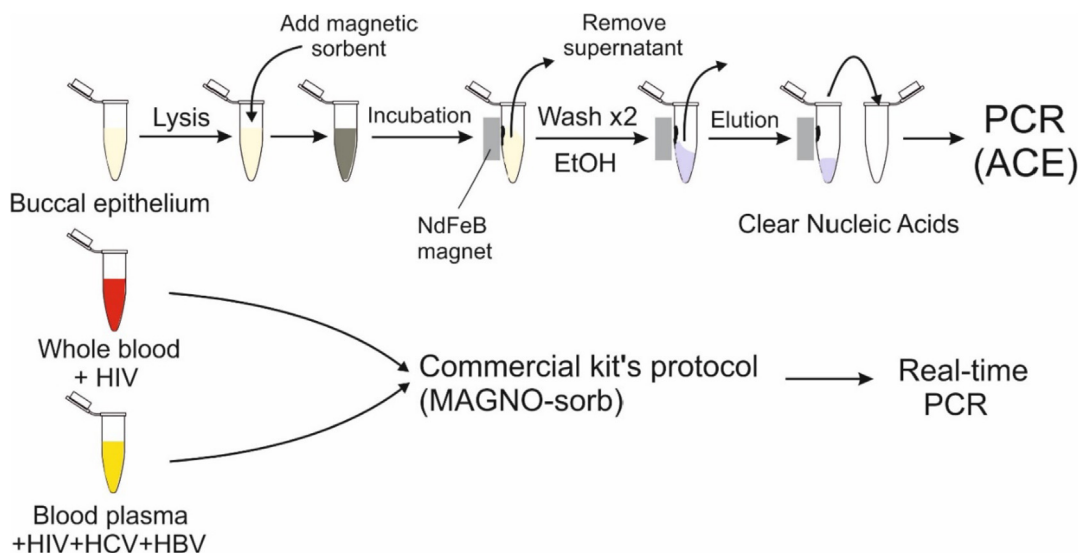


Fig. 2. Schematic illustration of the DNA isolation protocols.

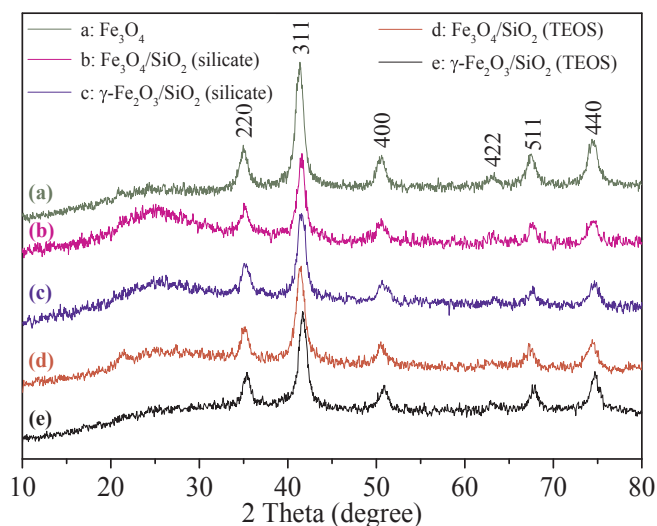


Fig. 3. XRD patterns of Fe_3O_4 (a), $\text{Fe}_3\text{O}_4/\text{SiO}_2$ and $\gamma\text{-Fe}_2\text{O}_3/\text{SiO}_2$ obtained via sodium silicate (b and c) and via TEOS (d and e) precursors.

at $\approx 20\text{--}30^\circ$. The lack of crystallinity is typical of silicon oxides obtained under similar conditions. Silica could remain amorphous up to the melting temperature [28,29]. This limits the possibilities of X-ray diffraction method when dealing with silicon oxides. The decreased intensity of spinel peaks in the XRD patterns of the MNCs as compared to bare Fe_3O_4 is caused by the presence of amorphous silica in the materials. Calcination at 750°C does not lead to significant coalescence or growth of iron oxide nanoparticles since diffraction peaks positions and their intensity remained unchanged. It could be the result of the presence of silica layers between the individual iron oxide nanoparticles in the MNC agglomerate, which limits the formation of contacts between iron oxide grains and internal diffusion [30,31]. The formation of silica framework is also possible inside the agglomerates, which prevents iron oxide nanoparticles from coalescence and imparts structural strength to the micron-sized agglomerates of the nanoparticles. In spite of a minor increase in the crystallinity, no structural changes were revealed by XRD analysis to occur under calcination at high temperatures up to 750°C . However, the color of all the MNCs samples changed to brown evidencing $\text{Fe}_3\text{O}_4 \rightarrow \gamma\text{-Fe}_2\text{O}_3$ transition. Note that the transformation of $\gamma\text{-Fe}_2\text{O}_3$ into the thermodynamically stable antiferromagnetic $\alpha\text{-Fe}_2\text{O}_3$ modification was not registered.

FTIR spectroscopy was used to complement the XRD results and to evaluate the surface state of the MNCs (Fig. 4). The IR spectroscopy results confirmed our assumption that the as prepared samples contain magnetite (Fe_3O_4) phase with a high symmetry of oxygen environment.

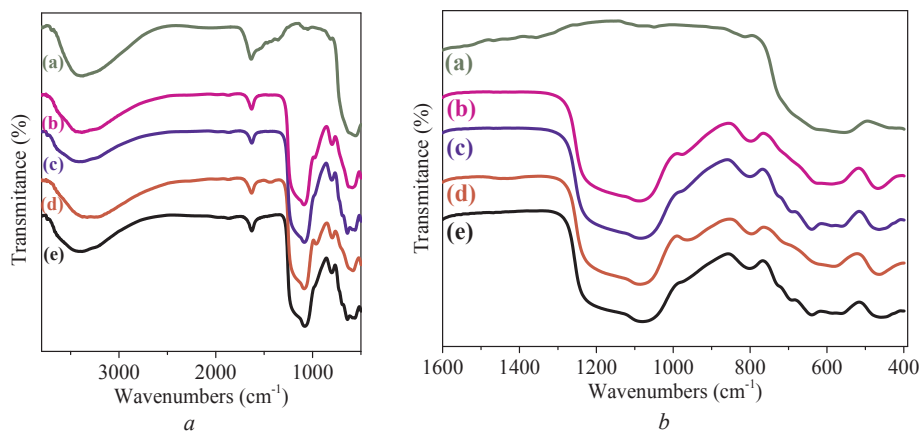


Fig. 4. Overview (a) and characteristic groups region (b) FTIR spectra of the synthesized samples: a – Fe_3O_4 ; b – $\text{Fe}_3\text{O}_4/\text{SiO}_2$ (via sodium silicate); c – $\gamma\text{-Fe}_2\text{O}_3/\text{SiO}_2$ (via sodium silicate); d – $\text{Fe}_3\text{O}_4/\text{SiO}_2$ (via TEOS); e – $\gamma\text{-Fe}_2\text{O}_3/\text{SiO}_2$ (via TEOS).

It resulted in two characteristic adsorption bands in the corresponding spectra. Thus, in the spectrum of individual magnetite (a), adsorption bands at 565 cm^{-1} and 400 cm^{-1} refer to Fe–O vibrations of spinel structure. These bands also appear in the spectra of the MNCs confirming the presence of iron oxide in the as prepared composites. The heating of the MNCs at $750\text{ }^\circ\text{C}$ leads to the oxidation of magnetite into maghemite ($\gamma\text{-Fe}_2\text{O}_3$) phase, which was reflected in the changes of the IR spectra (c, e). An emerging of new adsorption bands at 638 cm^{-1} and 588 cm^{-1} (the most intensive) indicates the formation $\gamma\text{-Fe}_2\text{O}_3$ having lower symmetry structure as compared to magnetite [32,33].

The broad band at 3380 cm^{-1} and the narrow band at 1629 cm^{-1} correspond to stretching and bending vibrations of O–H bonds of water adsorbed on the oxide surface.

The presence of silica on the surface of the MNCs can be proved by bond vibrations at 1086 cm^{-1} , 798 cm^{-1} and 464 cm^{-1} (b–e), which are specific for Si–O–Si [34]. The same intensity of the lines can be explained by the similar composition of the MNCs (b–e). The samples with the same compositions were synthesized to focus attention on the effect of different silica precursors and coating approaches on the properties of MNCs for bioseparation of NAs. The spectra of the MNCs obtained via TEOS are characterized by a higher intensity of Si–O–H silanol group vibrations at 974 cm^{-1} and 580 cm^{-1} as compared to the MNCs obtained via sodium silicate [34,35]. Nevertheless, after calcination at $750\text{ }^\circ\text{C}$, the silanol group signals of both samples become nearly equal. Thus, the thermal treatment neutralizes the effect of silica precursor nature on the structure of the resulting product. The indicated bands have a lower intensity in the spectra of calcined $\gamma\text{-Fe}_2\text{O}_3/\text{SiO}_2$ (c, e). This occurred due to dehydration processes, which result in a particular transformation of Si–O–H silanol groups into siloxane Si–O–Si groups or other structures with a lower dimension. The detailed mechanism of silanol group transformation was proposed by Zhuravlev [36].

The results of thermal analysis of the samples are shown in Fig. 5. The exothermic peaks at $143\text{ }^\circ\text{C}$ and $552\text{ }^\circ\text{C}$ for bare Fe_3O_4 nanoparticles are displaying oxidation of magnetite to maghemite and phase transformation of $\gamma\text{-Fe}_2\text{O}_3$ into $\alpha\text{-Fe}_2\text{O}_3$ (hematite), respectively [29]. It is important to emphasize that $\gamma\text{-Fe}_2\text{O}_3$ phase is characterized by an enhanced stability in the MNCs samples. The transition into anti-ferromagnetic $\alpha\text{-Fe}_2\text{O}_3$ phase does not occur even at $1000\text{ }^\circ\text{C}$ (duration is 12 h). This can be also proved by the absence of $\alpha\text{-Fe}_2\text{O}_3$ reflexes in the XRD patterns (Fig. 3) and the corresponding bands in the IR (Fig. 4) spectra, as well as the preservation of the magnetic characteristics of the MNCs. The effect of the increasing thermal stability of silica-encapsulated magnetite nanoparticles has already been studied [29,37]. This phenomenon allows thermal processing of the MNCs in a wide temperature range without loss in their magnetic properties. The weight losses of about 5.4 and 6.1% measured for samples b and d are attributed mostly to disposal of physically adsorbed and structure water. The higher mass loss of silica-derived samples can be explained

by their higher specific surface area and/or higher affinity of water for SiO_2 oxide.

Adsorption of inert gases on powders is a method giving valuable information on the state of surface, grain size and pore size distribution. The results of this method of characterization are useful for describing the adsorption on the solid/solution interface. It is seen from Fig. 6, that the MNCs prepared by both approaches demonstrate type IV nitrogen adsorption/desorption isotherm with small H3 type hysteresis loop occurred at relative pressure of 0.7–1.0. According to Brunauer–Emmett–Teller (BET) approximation of the adsorption isotherms, Na_2SiO_3 -derived MNCs (b) exhibits specific surface area of about $101\text{ m}^2/\text{g}$, which is higher than $67\text{ m}^2/\text{g}$ measured for TEOS-derived ones (d). The pore size distributions calculated by using Barrett–Joyner–Halenda (BJH) theory, are shown on the insert graph in Fig. 6. According to BJH analysis, the average pore diameters in Na_2SiO_3 -derived and TEOS-derived MNCs are 16.5 nm and 16.1 nm, respectively. However, the samples differ in the pore size distribution. Three regions of pores including microspores (1–2 nm), mesopores (15–25 nm) and large mesopores (~45 nm) have been identified. The large pores (42 nm) were related to the textural pores formed during the agglomeration of silica coated magnetite nanoparticles into micron-sized agglomerates. It is supposed that the large mesopores in the developed MNCs are mainly responsible for DNA sorption from water solution.

TEM micrograph of the uncoated Fe_3O_4 given in Fig. 7a shows the diameter of the grains to be in the range from 5 to 20 nm. The particles have a spherical shape with an average diameter of 8 nm. When no stabilizer is added to water suspension of bare Fe_3O_4 , the particles form agglomerates with an average hydrodynamic size of about 176 nm (measured by DLS technique, Fig. 7a). It is worth noting that the large hydrous shell of the oxide particles also contributes to the measured hydrodynamic diameter. The tendency of the particles to agglomerate is caused by their low zeta-potential (+18.2 mV) in neutral water solution. It was revealed that the magnetite agglomerates have only coagulation contacts and can be reversibly dispersed under ultrasonication with a peptizing agent. The MNC agglomerates have a size of about 1.5 μm and possess negative zeta-potential (around –26 mV) due to weakly acidic Si–O–H silanol groups of silica. The agglomerates remain structural stability due to a hard silica network embracing magnetite nanoparticles. The change of zeta-potential from positive to negative values also confirms successful encapsulation of magnetite particles with silica.

SEM images of the MNCs given in Fig. 8 show that the deposition of silica onto Fe_3O_4 nanoparticles results in large aggregates where the grains form a continuous spatial framework. The composites are evidently composed of Fe_3O_4 particles wrapped with SiO_2 coating. In order to reveal the effect of the silica precursor on the structural and functional properties of the materials, the conditions of the synthesis were selected to obtain the aggregates with nearly the same average diameter for the composites prepared via Na_2SiO_2 or TEOS silanizing reagents. In

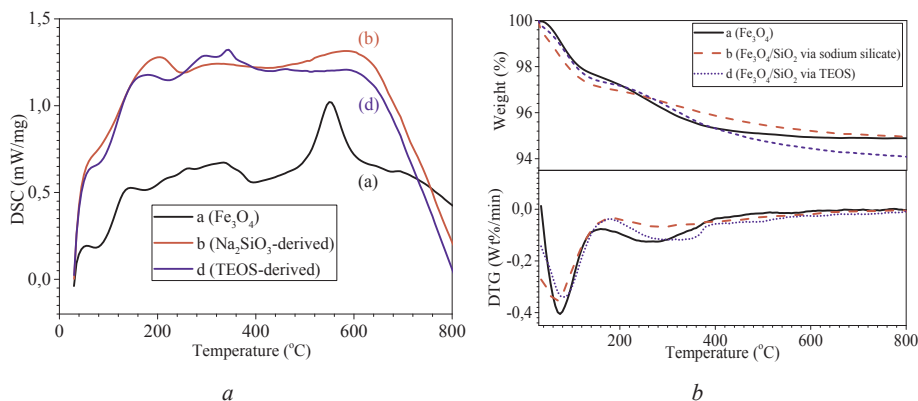


Fig. 5. DSC (a) and TG (b) curves of Fe_3O_4 and MNCs.

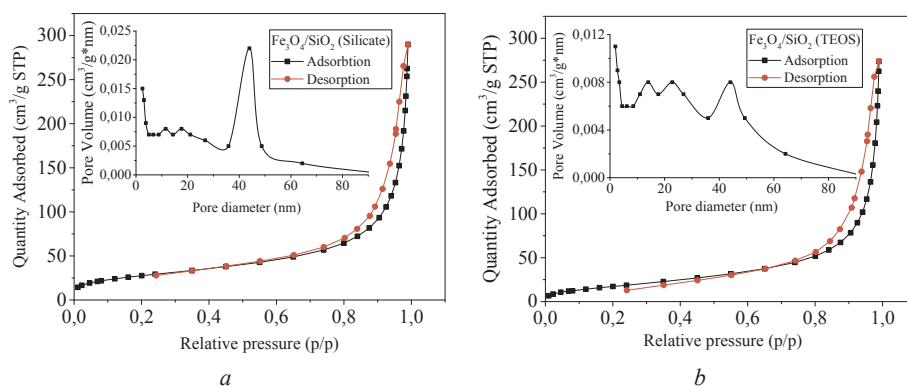


Fig. 6. Nitrogen adsorption/desorption isotherms on $\text{Fe}_3\text{O}_4/\text{SiO}_2$ nanocomposites obtained via sodium silicate (a) and TEOS (b). Insert graph: BJH pore size distribution.

contrast to Fe_3O_4 aggregates discussed above, both as prepared $\text{Fe}_3\text{O}_4/\text{SiO}_2$ aggregates consist of grains strongly bound with phase contacts within silica network. The hydrodynamic diameters of the Na_2SiO_3 - and TEOS-derived MNCs samples are about 1.3 and 1.7 μm , respectively (Fig. 9), which correlates with the SEM data. An additional ultrasonication of the suspensions does not lead to a noticeable change of the hydrodynamic size values due to silica network fastening the agglomerate. Note that under such treatment, nanoparticles with a size of 5–20 nm would have a tendency to form a stable sol. This would make impossible magnetic separation of the MNCs. Near micron-sized and structurally stable agglomerates are ideal candidates for biomolecules isolation due to intermediate colloidal stability in aqueous solutions. The SEM images acquired at low magnification (see Fig. 8) show no significant difference between $\text{Fe}_3\text{O}_4/\text{SiO}_2$ samples prepared via different silica precursors. Both the composites have a porous structure and irregularly shaped grains with a size ranging from 20 to 100 nm. The predominating diameter of the grains was estimated to be about 40 nm.

The synthesized magnetite nanoparticles have a high tendency to

agglomerate due to their high surface energy resulting from their small size and large specific surface area. The agglomeration leading to the decrease of their surface energy is a thermodynamically profitable process. There are many ways to prevent nanoparticles from agglomeration [38]. In our study, we exploited a controllable agglomeration to obtain near micron-sized particles with an intermediate colloidal stability. The size of agglomerates depends mostly on the diameter and surface features of the primary nanoparticles. The main particle surface parameter is zeta-potential. It might be controlled via solution parameters, such as pH, ionic strength, temperature, addition of coagulants and stabilizers etc. The effect of these parameters on iron oxide nanoparticles agglomeration have been previously reported in Refs. [39,40].

In the as prepared magnetite suspensions, the particles have strongly adsorbed layer of OH^- ions. The played a role of potential determining ions. However, the colloidal particles were electrically neutral (zeta-potential is close to zero) due to a high ionic strength of the solution containing high concentration of soluble salts. During the washing process, the dispersed system went through a maximum of aggregation stability. The removal of residual ions caused a decrease in

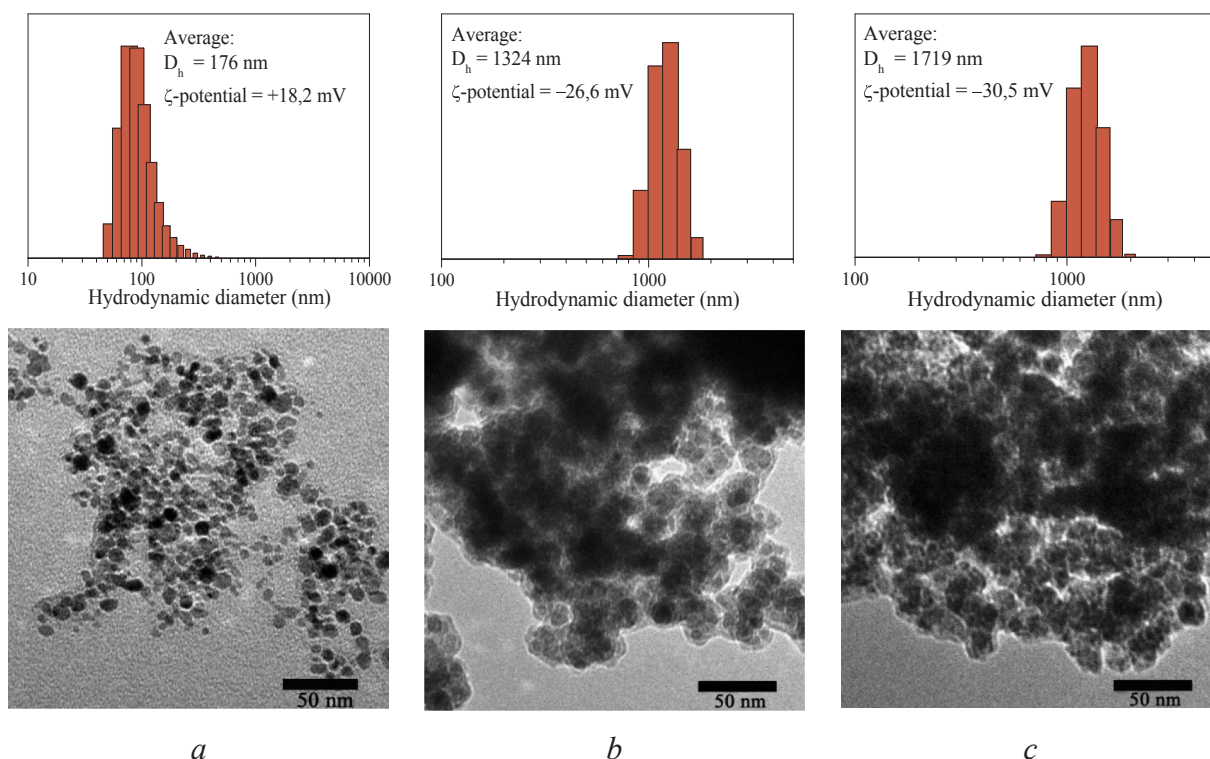


Fig. 7. TEM and DLC analysis of magnetite nanoparticles (a) and MNCs obtained via sodium silicate (b) and TEOS (c).

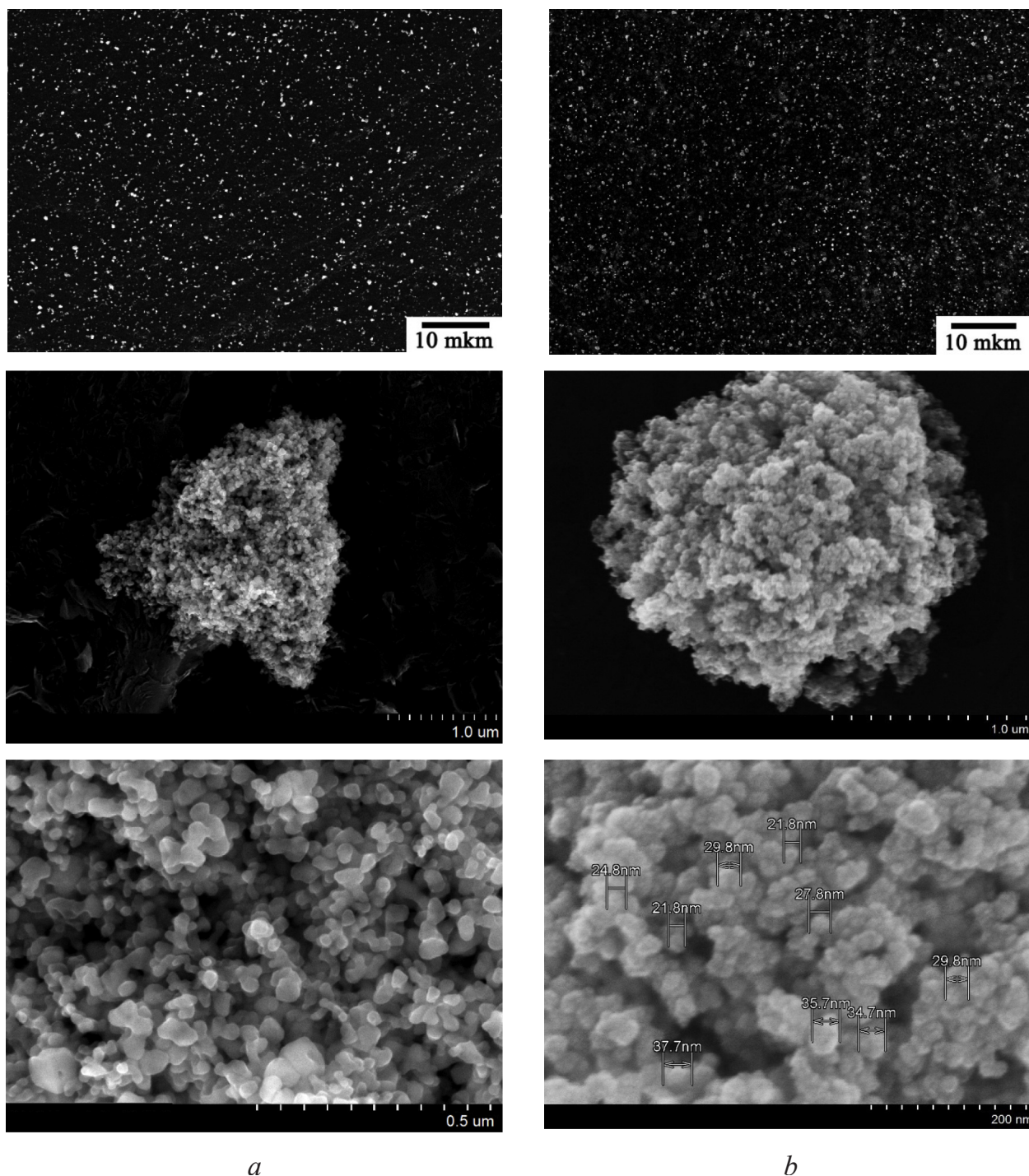


Fig. 8. SEM microphotographs of MNCs synthesized via sodium silicate (a) and TEOS (b) at three different magnifications.

the ionic strength of the solution and a growth of magnetite zeta-potential. In order to destabilize the colloidal solution formed, the washing steps had been repeated until the OH^- ions were desorbed. This resulted in an aggregation required for complete separation of the solid phase from the liquid.

The aggregation phenomenon was crucial at the salinization step, where the resulting particles were expected to lie in the range of $1 \div 3$ mkm. The reactants used at this step (concentrated NH_3 , Na_2SiO_3 and ethanol) act as typical coagulants and evoke total destabilization of the magnetite dispersions. In order to prevent uncontrollable agglomeration of the MNCs and keep the size of the resulting particle within the required range, the modes of stirring were varied. The optimal stirring

intensity was found to be around 300 rpm for dense-liquid process (Na_2SiO_3 precursor), and 400 rpm for Stöber method (TEOS precursor). Rather stable particles with a size about 1 mkm form when the hydrolysis of the silica precursors is over. The selected stirring rate caused the destruction of larger agglomerated. Silica matrix provides a high structural stability of the MNCs, especially in case of the samples calcined at high temperature. The obtained MNCs aggregates are strong enough to withstand an intensive ultrasonication.

As a rule, calcination at high temperature leads to leveling of all gender defects of the surfaces of solids resulting from synthesis features. In this case, similar decrease in average hydrodynamic size due to silica surface evolution was observed for both samples calcinated at 750°C

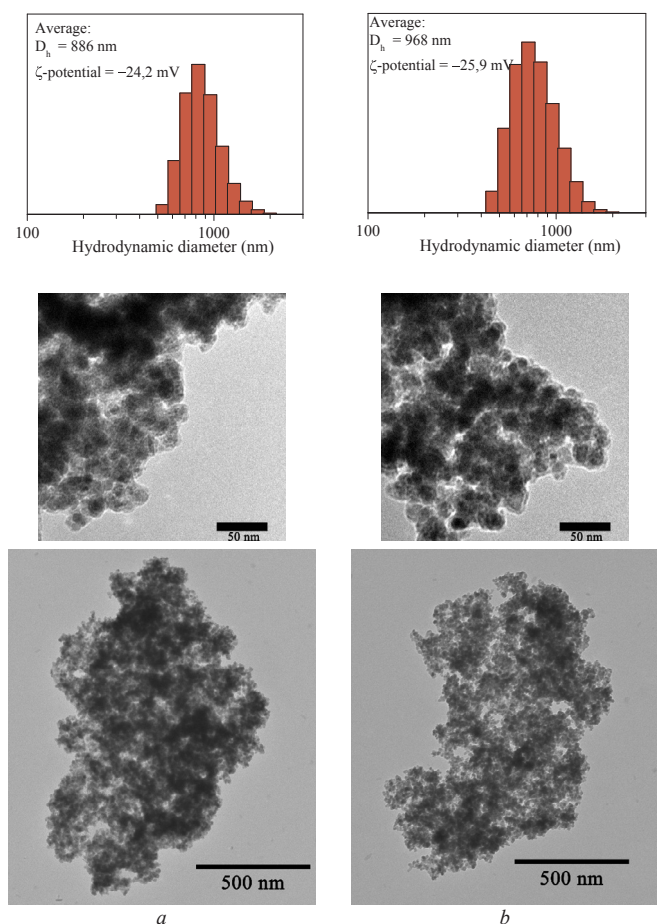


Fig. 9. DLC and TEM results of thermally treated (750 °C) γ - $\text{Fe}_2\text{O}_3/\text{SiO}_2$ samples obtained via sodium silicate (a) and TEOS (b).

(Fig. 9).

The driving force for the deposition of silica on the magnetite nanoparticles is adsorptive attraction between magnetite nanoparticles and siliceous micelles in the moment of their formation [41]. The formation of new solid phase of silica during sodium silicate or TEOS hydrolysis and polycondensation is more thermodynamically profitable on the magnetite nanoparticles possessing high surface energy, rather than in the bulk of solution. The resulting MNCs represent stable near micron-sized particles composed of small (20–40 nm) nanograins. Such material combines three features, important for bioseparation: intermediate colloidal stability of micron-sized particles (separability), high magnetization and superparamagnetism.

The room temperature (300 K) magnetization curves of all the samples are shown in Fig. 10. The magnetization at field of 40 kOe was taken as a saturation magnetization (M_{sat}). The expected decrease in M_{sat} from 67.6 emu/g for bare Fe_3O_4 to about 42 emu/g for the MNC is proportional to diamagnetic SiO_2 content. Thus, the silica encapsulation does not lead to a change in magnetic state of individual Fe_3O_4 nanoparticles. The relatively high magnetization values of the MNCs and their micron-sized state lead to a short time required for complete separation and immobilization of the MNC particles.

In case of neutral water suspension (5 mg/mL solid phase) and permanent neodymium magnet, the time of separation is less than 60 s, which is appropriate for the technological process. The observed fast magnetic response and the formation of clear solution after isolation of sorbents are essential requirements of the MNC to be used for bioseparation.

3.2. Isolation and characterization of nucleic acids

At the first step of the validation of the synthesized materials, non-specific NAs isolation from human buccal epithelium cells of two different donors was carried out. According to the UV spectroscopy data of the isolated NAs, an average relation of UV adsorption spectra at 260 nm and 280 nm (A_{260}/A_{280}) of the samples is 1.94. This value is higher than 1.80, the generally accepted standard of pure genomic DNA [42]. A higher A_{260}/A_{280} value can be explained by the presence of RNA in the isolated NAs mixture ($A_{260}/280$ for RNA is 2.0) because RNase A has not been used in our protocol. The obtained A_{260}/A_{230} ratio, which is commonly higher than $A_{260}/280$, is lower than $A_{260}/280$ in our study indicating a slight guanidine hydrochloride contamination. Despite this fact, an inhibition of the following PCR assay has not occurred due to very small content of impurities. The average concentrations of the isolated samples (elution in 200 μL) are 55.1, 45.9, 48.4, and 39.4 ng/ μL for b, c, d, and e magnetic sorbents, respectively. This corresponds to isolation efficiencies of 11.0, 9.2, 9.7 and 7.9 mg (NAs)/g (sorbent) for b, c, d, and e, respectively for a typical routine NAs isolation from a model biosample. Although there is no significant difference between the resulting concentrations, it can be noted that the thermally treated MNCs isolate slightly less NAs with higher A_{260}/A_{280} value: from 1.87 to 1.95 after calcination of silicate-derived MNCs and from 1.90 to 1.99 after calcination of TEOS-derived MNCs. Actually, the concentrations of isolated NA depend highly on samples collection procedures. Nevertheless, the method generally allows magnetic sorbent to isolate enough NAs (DNA and RNA mix) required for a typical test in medical diagnostics.

According to the adsorption experiments with salmon genomic DNA samples, silica derived $\text{Fe}_3\text{O}_4/\text{SiO}_2$ possesses a higher adsorption capacity (82.5 mg/g) compared to TEOS-derived one (64.3 mg/g), that can be explained by their higher surface area (101 vs 67 m^2/g). Calcination of the MNCs at 750 °C leads to a significant decrease of their DNA adsorption capacity: from 82.5 to 46.9 mg/g for silica-derived MNCs, and from 64.3 to 45.0 mg/g for TEOS-derived MNCs. This could be related with the decrease in both silanol groups concentration on the oxide surface and specific surface area of the MNCs. The latter effect was already discussed above. It is worth noting that the calcinated MNCs (samples c and e) desorb nucleic acids considerably more readily than the uncalcinated ones (samples b and d), which should be taken into account in DNA isolation experiments. Thus, the calcination caused the average DNA desorption rates to increase from 66.0 to 85.9% during the first elution step. In spite of the decrease in the adsorption capacity, higher desorption rates benefit for analytical applications involving extremely small amounts of target DNA (medical and forensic diagnostics). It is important to add that the features of various MNCs can be compared properly only within the same isolation protocol. The increase in the MNCs performance can be achieved via further tuning the DNA isolation protocol parameters (chemical composition, concentrations, pH, temperature etc.).

In our study, ACE I/D polymorphism PCR assay played a role of a model molecular biology application [43]. Generally, ACE gene codes angiotensin-1 converting enzyme, presenting a significant part of the renin-angiotensin system that controls blood pressure by regulating body fluid levels. ACE I/D polymorphism was one of the first genetic factor to be described and associated with human physical performance. The ACE I allele (produced 490 bp fragments) is consistently associated with endurance performance and higher exercise efficiency while the D allele (190 bp fragments) is associated with strength and power performance [44]. The results of agarose gel electrophoresis of PCR amplification products are given in Fig. 11. Lanes M and N are related to molecular weight marker (100–1000 bp) and negative control (distilled water) of PCR amplification without DNA template respectively. Lanes 1 and 2, 3 and 4, 5 and 6, 7 and 8 are PCR amplification products of NA samples isolated with b, c, d and e nanocomposites, respectively. It is evident that the chosen donors

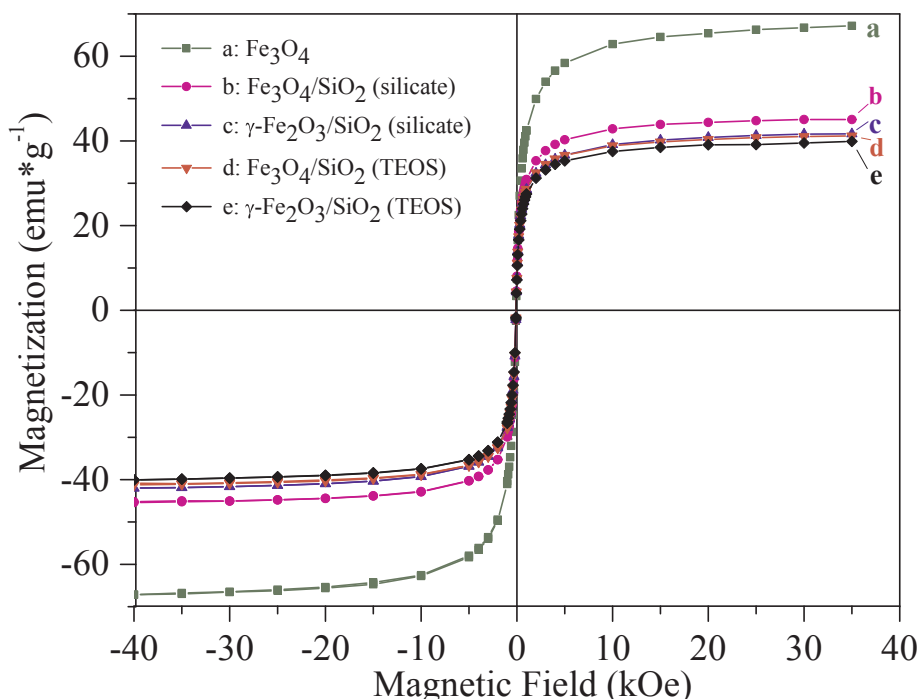


Fig. 10. Room temperature magnetization curves of the synthesized MNCs.

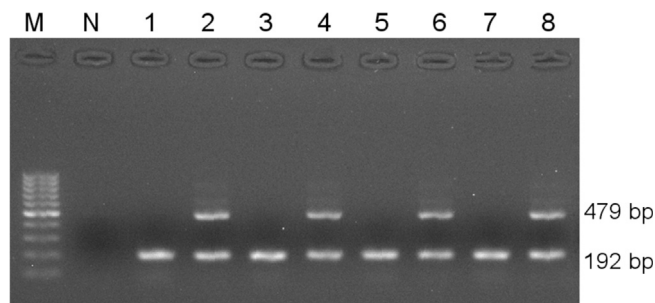


Fig. 11. ACE I/D polymorphism detection PCR assay of nucleic acids isolated with the synthesized MNCs.

possess different genotype of ACE gen: odd lanes (1, 3, 5, 7) correspond to D/D genotype donor and even lanes (2, 4, 6, 8) to I/D genotype donor. All the samples isolated via *b* and *c* MNCs gave clear and bright amplification patterns (1–8) without amplification failure. The bands in lanes 1–8 have nearly the same brightness, indicating that they may have similar concentrations of PCR products, as the result of similar DNA concentrations of the samples after the isolation. This data reveal that the synthesized MNCs are suitable for isolation and following PCR analysis of DNA from buccal epithelium cells.

At the second step of the practical validation, the synthesized MNCs

have been compared with commercially available MAGNO-sorb® total NAs isolation kit (InterLabService, Russia) in a model diagnostic application – HBV-HCV-HIV test. Internal control gene (ICS) sample was used to confirm that the RT-PCR process is proceeding well. The obtained threshold cycle (*Ct*) values presented in Table 1 are quite similar.

Minor differences between the synthesized MNCs and the reference seen from Table 1 are not significant. In some cases, they are even less than the average absolute deviations of measurements. It is important to note that the main tendency of RNA content to increase after thermal treatment of MNCs also manifests itself in viral analysis. The higher quantity of isolated viral RNA is reflected in decreasing *Ct* values of samples *c* and *e* as compared to *b* and *d*. HIV and HCV have a genetic material inside the presented viral RNA. The increase in the effectiveness of the viral NA isolation with the calcined MNC can be explained by their lower surface activity providing better desorption of NAs. In spite of the decrease in the adsorption capacity, the calcination lead to the growth of desorption rate due to lower surface area and lower amount of surface silanol groups in the calcined MNCs, which facilitates the NAs desorption. All the above indicates the possibility of sodium silicate to be used for the synthesis of magnetic sorbents comparable with TEOS-derived ones.

4. Conclusions

Micron-sized $\text{Fe}_3\text{O}_4/\text{SiO}_2$ and $\gamma\text{-Fe}_2\text{O}_3/\text{SiO}_2$ particles prepared via

Table 1

The results of RT-PCR assay of viral NAs isolated via the synthesized nanocomposites and the commercial MAGNO-sorb® isolation kit.

RT-PCR/Sorbent	Viral RNA in human whole blood			Viral NAs in human blood plasma		
	Ct value					
	β -globin	HIV	HBV	HCV	HIV	ICG
MAGNO-sorb®	17.54 ± 0.54	23.80 ± 0.38	25.81 ± 0.26	27.76 ± 0.08	28.42 ± 0.48	23.79 ± 0.16
<i>b</i>	17.99 ± 0.90	23.34 ± 0.34	26.49 ± 0.25	28.67 ± 0.23	29.65 ± 0.47	24.57 ± 0.12
<i>c</i>	17.60 ± 0.96	23.27 ± 0.30	25.97 ± 0.13	28.04 ± 0.23	28.99 ± 0.17	24.21 ± 0.11
<i>d</i>	18.47 ± 0.93	23.52 ± 0.15	26.43 ± 0.09	28.44 ± 0.19	29.50 ± 0.38	24.54 ± 0.05
<i>e</i>	17.92 ± 1.15	23.63 ± 0.15	26.18 ± 0.17	27.98 ± 0.29	29.46 ± 0.44	24.54 ± 0.10

two facile methods involving different silica precursors were systematically studied and employed for nucleic acids isolation and analysis. The effect of silica precursor nature (Na_2SiO_3 and TEOS) and calcination (750°C) on the structural features and NAs isolation performance of the MNCs prepared under similar conditions has been revealed. It was found that the as prepared MNCs represent large agglomerates ($\sim 1.5 \mu\text{m}$) consisting of nanosized (20–100 nm) iron oxide and silica nanoparticles bound together with strong phase contacts. The differences in the specific surface area and pore size distributions were revealed for the MNCs obtained via Na_2SiO_3 and TEOS, which is likely related to different mechanisms of the SiO_2 -precursor hydrolysis. A higher specific surface area was measured for Na_2SiO_3 -derived MNCs ($101 \text{ m}^2/\text{g}$ vs $67 \text{ m}^2/\text{g}$ for TEOS-derived sample). Also, in case of Na_2SiO_3 precursor, large mesopores ($\sim 45 \text{ nm}$) predominate in the structure of the MNCs. They are related to the textural pores generated during the agglomeration of oxide nanoparticles.

IR spectroscopy method allowed revealing fine structural distinctions between samples that were not detected by XRD analysis. Thus, the concentration of silanol groups ($\text{Si}-\text{OH}$) were found to be higher for the MNCs obtained via TEOS as compared to Na_2SiO_3 -derived ones. However, calcination of both the powdered samples at 750°C leads to the equalization of the corresponding IR absorption bands. Thus, thermal treatment compensates the effect of SiO_2 -precursor nature on the structure of the MNCs.

Thermal treatment of the as prepared $\text{Fe}_3\text{O}_4/\text{SiO}_2$ powders at $\sim 160^\circ\text{C}$ leads to $\text{Fe}_3\text{O}_4 \rightarrow \gamma\text{-Fe}_2\text{O}_3$ transition within the MNCs, while the agglomerate size and pore size distribution remain nearly unchanged for both the samples. Such treatment is advisable for the studied materials to provide their long-term stability.

Calcination at temperatures up to 1000°C for 12 h does not evoke $\gamma\text{-Fe}_2\text{O}_3$ transition into antiferromagnetic $\alpha\text{-Fe}_2\text{O}_3$ phase due to stabilizing effect of SiO_2 matrix. Thus, the structural and functional properties of the MNCs can be tailored by varying the conditions of heat treatment over a wide range of temperatures. Along with nearly micron size and structural stability of the agglomerates, the prepared MNCs are characterized by superparamagnetic behavior and rather high magnetization ($\sim 40 \text{ emu/g}$).

The developed $\text{Fe}_3\text{O}_4/\text{SiO}_2$ and $\gamma\text{-Fe}_2\text{O}_3/\text{SiO}_2$ nanocomposite particles were shown as a valuable tool for NAs isolation from biological samples in microscale and preparative purification procedure. The isolated and purified NAs samples were suitable for genotyping and RT-PCR analysis of viral particles (HCV, HBV, HIV). Therefore, the synthesized particles are suitable for molecular diagnostic system as well as for forensic applications.

Acknowledgements

The authors are grateful to Kononov A.S. (JSC «NextBio», Moscow, Russian Federation) for the preparation of viral samples and RT-PCR assay.

References

- [1] A.V. Trukhanov, S.V. Trukhanov, V.G. Kostishyn, et al., Microwave properties of the Ga-substituted $\text{BeFe}_{12}\text{O}_{19}$ hexaferrites, *Mater. Res. Express* 4 (2017) 076106, <https://doi.org/10.1088/2053-1591/aa50b9>.
- [2] C. Jiang, Y. Sun, X. Yu, et al., Removal of Sudan dyes from water with C_{18} -functional ultrafine magnetic silica nanoparticles, *Talanta* 89 (2012) 38–46, <https://doi.org/10.1016/j.talanta.2011.11.052>.
- [3] J. He, M. Huang, D. Wang, Magnetic separation techniques in sample preparation for biological analysis: a review, *J. Pharmaceut. Biomed. Anal.* 101 (2014) 84–101, <https://doi.org/10.1016/j.jpba.2014.04.017>.
- [4] L. Xie, R. Jiang, F. Zhu, et al., Application of functionalized magnetic nanoparticles in sample preparation, *Anal. Bioanal. Chem.* 406 (2014) 377–399, <https://doi.org/10.1007/s00216-013-7302-6>.
- [5] Yu.V. Bogachev, A.V. Nikitina, A.A. Kostina, et al., NMR relaxation efficiency of aqueous solution of composite $\text{M}_x\text{Zn}_y\text{Fe}_{3-x-y}\text{O}_4$ nanoparticles, *Appl. Magn. Reson.* 48 (2017) 715–722, <https://doi.org/10.1007/s00723-017-0889-6>.
- [6] L.H. Reddy, J.L. Arias, J. Nicolas, et al., Magnetic nanoparticles: design, characterization, toxicity and biocompatibility, pharmaceutical and biomedical applications, *Chem. Rev.* 112 (2012) 5818–5878, <https://doi.org/10.1021/cr300068p>.
- [7] N.Z. Knezevic, E. Ruiz-Hernandez, W.E. Hennink, M. Vallet-Regi, Magnetic mesoporous silica-based core/shell nanoparticles for biomedical applications, *RSC Adv.* 3 (2013) 9584–9593, <https://doi.org/10.1039/c3ra23127e>.
- [8] S.C. Tan, B.C. Yiap, DNA, RNA, and protein extraction: the past and the present, *J. Biomed. Biotechnol.* 2009 (2009) 10, <https://doi.org/10.1155/2009/574398>.
- [9] A.S. Hutchins, M.J. Astwood, J.R. Saah, et al., Evaluation of automated and manual DNA purification methods for detecting *Ricin* communis DNA during ricin investigations, *Forensic Sci. Int.* 236 (2014) 10–15, <https://doi.org/10.1016/j.forsciint.2013.12.011>.
- [10] R. Boom, C.J.A. Sol, M.M.M. Salimans, et al., Rapid and simple method for purification of nucleic acids, *J. Clin. Microbiol.* 28 (1990) 495–503 0095-1137/90/030495-09\$02.00/0.
- [11] C.-L. Chiang, C.-S. Sung, C.-Y. Chen, Application of silica-magnetite nanoparticles to the isolation of ultrapure plasmid DNA from bacterial cells, *J. Magn. Magn. Mater.* 305 (2006) 483–490, <https://doi.org/10.1016/j.jmmm.2006.02.088>.
- [12] X. Li, J. Zhang, H. Gu, Adsorption and desorption behaviors of DNA with magnetic mesoporous silica nanoparticles, *Langmuir* 27 (2011) 6099–6106, <https://doi.org/10.1021/la104653s>.
- [13] I.J. Bruce, J. Taylor, M. Todd, et al., Synthesis, characterization and application of silica-magnetite nanocomposites, *J. Magn. Magn. Mater.* 284 (2004) 145–160, <https://doi.org/10.1016/j.jmmm.2004.06.032>.
- [14] E. Taboada, R. Solanas, E. Rodriguez, et al., Supercritical-fluid-assisted one-pot synthesis of biocompatible core($\gamma\text{-Fe}_2\text{O}_3$)/shell(SiO_2) nanoparticles as high relaxivity T_2 -contrast agents for magnetic resonance imaging, *Adv. Funct. Mater.* 19 (2009) 2319–2324 0.1002/adfm.200801681.
- [15] H.L. Ding, Y.X. Zhang, S. Wang, et al., $\text{Fe}_3\text{O}_4/\text{SiO}_2$ core/shell nanoparticles: the silica coating regulations with a single core for different core sizes and shell thickness, *Chem. Mater.* 24 (2012) 4572–4580, <https://doi.org/10.1021/cm302828d>.
- [16] R. Fu, X. Jin, J. Liang, et al., Preparation of highly monodispersed $\text{Fe}_3\text{O}_4/\text{SiO}_2$ composite particles from aggregates of Fe_3O_4 nanoparticles, *J. Mater. Chem.* 21 (2011) 15352–15356, <https://doi.org/10.1039/c1jm11883h>.
- [17] I.J. Bruce, T. Sen, Surface modification of magnetic nanoparticles with alkoxysilanes and their application in magnetic bioseparation, *Langmuir* 21 (2005) 7029–7035, <https://doi.org/10.1021/la050553t>.
- [18] W. Stober, A. Fink, E. Bohn, Controlled growth of monodisperse silica spheres in the micron size range, *J. Colloid Interface Sci.* 26 (1968) 62–69, [https://doi.org/10.1016/0021-9797\(68\)90272-5](https://doi.org/10.1016/0021-9797(68)90272-5).
- [19] W. Wang, W. Shan, H. Ru, Facile preparation and new formation mechanism of plugged SBA-15 silicas based on cheap sodium silicate, *J. Mater. Chem.* 21 (2011) 17433–17440, <https://doi.org/10.1039/c1jm13669k>.
- [20] J. Kim, J. Lee, J.-W. Choi, et al., Synthesis and characterization of hollow silica particles from tetraethyl orthosilicate and sodium silicate, *J. Nonosci. Nanotechnol.* 13 (2013), <https://doi.org/10.1166/jnn.2013.7074> 2284–2288.
- [21] N. Ya, Y. Gong, D. Wu, et al., One-pot synthesis of mesoporous organosilicas using sodium silicate as a substitute for the tetraalkoxysilane, *Microporous Mesoporous Mater.* 72 (2004) 25–32, <https://doi.org/10.1016/j.micromeso.2004.04.013>.
- [22] X. Pang, F. Tang, Morphological control of mesoporous materials using inexpensive silica sources, *Microporous Mesoporous Mater.* 85 (2005) 1–6, <https://doi.org/10.1016/j.micromeso.2005.06.012>.
- [23] Q. Liu, Z. Xu, J.A. Finch, et al., A novel two-step silica-coating process for engineering magnetic nanocomposites, *Chem. Mater.* 10 (1998) 3936–3940, <https://doi.org/10.1021/cm980370a>.
- [24] A. Jitianu, M. Raileanu, M. Crisan, et al., $\text{Fe}_3\text{O}_4\text{-SiO}_2$ nanocomposites obtained via alkoxide and colloidal route, *J. Sol. Gel Sci. Technol.* 40 (2006) 317–323, <https://doi.org/10.1007/s10971-006-9321-7>.
- [25] N. Sun, C. Deng, X. Zhao, et al., Extraction of total nucleic acids based on silica-coated magnetic particles for RT-qPCR detection of plant RNA virus/viroid, *J. Virol. Methods* 196 (2014) 204–211, <https://doi.org/10.1016/j.jviromet.2013.11.012>.
- [26] R. Massart, Preparation of aqueous magnetic liquids in alkaline and acidic media, *IEEE Trans. Magn.* 17 (1981) 1247–1248 0018-9464/81/0300-1248\$00.75.
- [27] Y.-H. Deng, C.-C. Wang, J.-H. Hu, et al., Investigation of formation of silica-coated magnetite nanoparticles via sol-gel approach, *Colloids. Surf. A Physicochem. Eng. Asp.* 262 (2005) 87–93, <https://doi.org/10.1016/j.colsurfa.2005.04.009>.
- [28] M. Helmi Rashid Firimani, N. Shahtahmasebi, M. Rezaee Roknabadi, et al., Study of structural and magnetic properties of superparamagnetic $\text{Fe}_3\text{O}_4/\text{SiO}_2$ core-shell nanocomposites synthesized with hydrophilic citrate-modified Fe_3O_4 seeds via a sol-gel approach, *Physica E Low. Dimens. Syst. Nanostruct.* 53 (2013) 207–216, <https://doi.org/10.1016/j.physe.2013.04.032>.
- [29] F. Fajaroh, H. Setyawan, A. Nur, et al., Thermal stability of silica-coated magnetite nanoparticles prepared by an electrochemical method, *Adv. Powder Technol.* 24 (2013) 507–511, <https://doi.org/10.1016/j.apt.2012.09.008> 10.1016/j.apt.2012.09.008.
- [30] G. Ennas, A. Musinu, G. Piccaluga, et al., Characterization of iron oxide nanoparticles in an $\text{Fe}_2\text{O}_3\text{-SiO}_2$ composite prepared by a sol-gel method, *Chem. Mater.* 10 (1998) 495–502, <https://doi.org/10.1021/cm970400u>.
- [31] C. Liu, A. Wang, H. Yin, et al., Preparation of nanosized hollow silica spheres from SiO_2 using Fe_3O_4 nanoparticles as templates, *Particuology* 10 (2012) 352–358, <https://doi.org/10.1016/j.partic.2011.04.009>.
- [32] J. Murbe, A. Rechtenbach, J. Topfer, Synthesis and physical characterization of magnetite nanoparticles for biomedical applications, *Mater. Chem. Phys.* 110 (2008) 426–433, <https://doi.org/10.1016/j.matchemphys.2008.02.037>.

- [33] Y.-S. Li, J.S. Church, A.L. Woodhead, Infrared and Raman spectroscopic studies on iron oxide magnetic nano-particles and their surface modifications, *J. Magn. Magn Mater.* 324 (2012) 1543–1550, <https://doi.org/10.1016/j.jmmm.2011.11.065>.
- [34] P. Innocenzi, Infrared spectroscopy of sol-gel derived silica-based films: a spectro-microstructure overview, *J. Non-Cryst. Solids* 316 (2003) 309–319, [https://doi.org/10.1016/S0022-3093\(02\)01637-X](https://doi.org/10.1016/S0022-3093(02)01637-X).
- [35] J.R. Martinez, F. Ruiz, Y.V. Vorobiev, et al., Infrared spectroscopy analysis of the local atomic structure in silica prepared by sol-gel, *J. Chem. Phys.* 109 (1998) 7511, <https://doi.org/10.1063/1.477374>.
- [36] L.T. Zhuravlev, The surface chemistry of amorphous silica. Zhuravlev model. *Colloids Surf A Physicochem Eng Asp*, 173(200) 1–38, 10.1016/S0927-7757(00)00556-2.
- [37] A.E. Panasenko, I.A. Tkachenko, L.A. Zemnukhova, et al., Phase composition, magnetic properties and thermal behavior of a novel Fe₂O₃-SiO₂ composite material, *J. Magn. Magn Mater.* 405 (2016) 66–71, <https://doi.org/10.1016/j.jmmm.2015.11.087>.
- [38] P.J. Vikesland, et al., Aggregation and sedimentation of magnetite nanoparticle clusters, *Environ Sci Nano* 3 (2016) 567–577, <https://doi.org/10.1039/C5EN00155B>.
- [39] K. Shimizu, S.V. Sokolov, R.G. Compton, Agglomeration equilibria of hematite nanoparticles, *Colloid and Interface Science Communications* 13 (2016) 19–22, <https://doi.org/10.1016/j.colcom.2016.06.003>.
- [40] E. Demangeat, et al., Colloidal and chemical stabilities of iron oxide nanoparticles in aqueous solutions: the interplay of structural, chemical and environmental drivers, *Environ. Sci. Nano* 5 (2018) 992–1001, <https://doi.org/10.1039/C7EN01159H>.
- [41] L. Chen, Z. Xu, H. Dai, et al., Facile synthesis and magnetic properties of mono-disperse Fe₃O₄/Silica nanocomposite microstructures with embedded structures via direct solution-based route, *J. Alloy. Comp.* 497 (2010) 221–227, [https://doi.org/10.1016/S0927-7757\(00\)00556-2](https://doi.org/10.1016/S0927-7757(00)00556-2).
- [42] P. Desjardins, NanoDrop microvolume quantitation of nucleic acids, *J. Vis. Exp.* 45 (2010) 2565, <https://doi.org/10.3791/2565>.
- [43] F.A. Styed-Tabatabaei, B.A. Oostra, A. Isaacs, et al., ACE polymorphisms, *Circ. Res.* 98 (2006) 1123–1133, <https://doi.org/10.1161/01.RES.0000223145.74217.e7>.
- [44] Y.P. Pitsiladis, M. Tanaka, N. Eynon, et al., Athlome Project Consortium: a concerted effort to discover genomic and other "omic" markers of athletic performance, *Physiol. Genom.* 48 (2016) 183–190, <https://doi.org/10.1152/physiolgenomics.00105.2015>.